

## Hydroconversion of Oxidation Products of Sulfur-Containing Aromatic Compounds

A. V. Vutolkina<sup>a,\*</sup>, A. V. Akopyan<sup>a</sup>, A. P. Glotov<sup>b</sup>, M. S. Kotelev<sup>b</sup>,  
A. L. Maksimov<sup>a,c</sup>, and E. A. Karakhanov<sup>a</sup>

<sup>a</sup> Moscow State University, Moscow, 119991 Russia

<sup>b</sup> Gubkin Russian State University of Oil and Gas (Natural Research University), Moscow, 119991 Russia

<sup>c</sup> Topchiev Institute of Petrochemical Synthesis, Russian Academy of Sciences, Moscow, 119991 Russia

\*e-mail: annavutolkina@mail.ru

Received June 5, 2018

**Abstract**—Hydroconversion of benzo- and dibenzothiophene sulfone on a Ni–Mo sulfide catalyst based on mesoporous aluminosilicate Al-HMS and on unsupported catalysts prepared in situ in the course of decomposition of poorly soluble precursors (molybdenum hexacarbonyl, nickel naphthenate) was studied. Hydrogenation of sulfones was performed at 250, 340, and 380°C and elevated CO pressure in the presence of water ensuring in situ generation of hydrogen via water-gas shift reaction.

**DOI:** 10.1134/S1070427218060162

Environmental standards prohibiting sale of motor fuels with high sulfur content become more and more stringent, which stimulates the improvement of oil refining technologies with the aim of considerably reducing the sulfur content of hydrocarbon fractions. In the past several years, there has been a great deal of interest in the development not only of high-performance catalysts, but also of novel complex, economically efficient, and highly productive technologies for reducing the total sulfur content (down to 0.001 wt % inclusive) in oil refining products and in the pretreatment steps without using hydrogen.

Oxidative desulfurization seems to be the most promising procedure for removing sulfur compounds. The following oxidants can be used: H<sub>2</sub>O<sub>2</sub>, HNO<sub>3</sub>, N<sub>2</sub>O, NaClO, NaClO<sub>2</sub>, NaBrO, C<sub>5</sub>H<sub>11</sub>NO<sub>2</sub>, NaIO<sub>4</sub>, various alkyl hydroperoxides, molecular oxygen, or air [1, 2]. These reactions are catalyzed, as a rule, by transition metal compounds such as vanadium pentoxide, sodium molybdate and tungstate, or peroxotungstate complexes, with lower carboxylic acids as cocatalysts [3–7]. Oxidative desulfurization allows reaching very low sulfur content of petroleum products with the removal of benzothiophene and dibenzothiophene, which exhibit low reactivity under the hydrotreating conditions, by

their oxidation to the corresponding sulfoxides and sulfones [8, 9]. The oxidation products are removed by adsorption or extraction with polar organic solvents [10, 11].

The key problem in performing oxidative desulfurization is the influence exerted by oxidation products remaining in the hydrocarbon fraction after the adsorption or extraction treatment on the properties of the fraction being treated and on the subsequent processes, in particular, on those involving hydrogen. To determine how “residual” sulfones affect the subsequent hydroprocessing, we prepared model hydrocarbon mixtures containing benzo- and dibenzothiophene sulfones, after which we performed desulfurization using Ni–Mo sulfide catalysts, both supported and formed in the course of thermal decomposition of poorly soluble precursors, in the CO/H<sub>2</sub>O system.

As support for Ni–Mo sulfide catalysts we used mesoporous aluminosilicate Al-HMS-10. Catalysts based on it have high specific surface area and the pore size ensuring the substrate access to the active component. Unsupported dispersed catalysts formed by thermal decomposition of metal salts in the presence of sulfiding agent are characterized by high content of

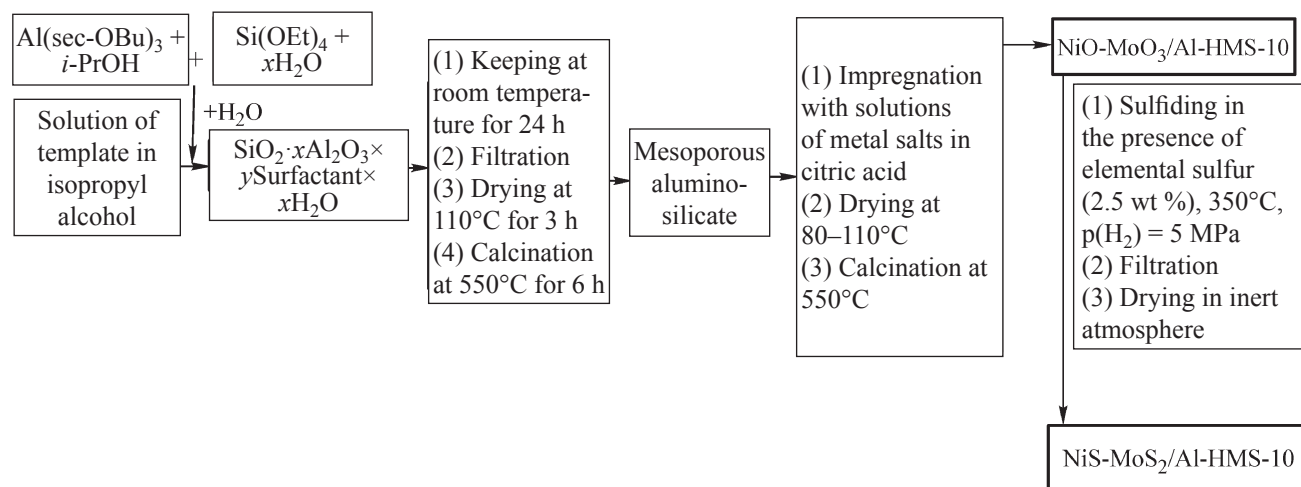


Fig. 1. Scheme of the synthesis of mesoporous aluminosilicate Al-HMS and of the Ni-Mo sulfide catalyst based on it.

the active phase. In addition, the use of these catalytic systems virtually eliminates the effect of steric and diffusion factors hindering the substrate access to the catalyst active component, which makes these systems highly active in hydrogenation.

## EXPERIMENTAL

**Preparation of benzo- and dibenzothiophene sulfones.** As starting compounds we used toluene (ultrapure grade, Reakhim, Russia), benzothiophene (98%, Alfa Aesar), dibenzothiophene (98%, Sigma-Aldrich), hydrogen peroxide (50%, Prime Chemicals Group), and formic acid (88%, chemically pure grade, Komponent-Reaktiv, Russia).

A temperature-controlled reactor was charged with n-octane. The starting benzothiophene or dibenzothiophene was added in an amount corresponding to the 5000 ppm concentration. After its dissolution, a 50% hydrogen peroxide solution was added in an amount corresponding to the molar ratio  $\text{H}_2\text{O}_2 : \text{S} = 10 : 1$ . Formic acid taken in the molar ratio  $\text{HCOOH} : \text{S} = 5 : 1$  was used as a catalyst. The mixture was stirred for 2 h at  $60^\circ\text{C}$ . The precipitate was filtered off, washed with excess n-hexane, and dried on a rotary evaporator to constant weight. The benzo- and dibenzothiophene sulfones obtained were analyzed by GLC and  $^1\text{H}$  NMR.

**Synthesis of catalysts supported on mesoporous aluminosilicate Al-HMS.** Figure 1 shows the scheme of the synthesis of the Ni-Mo sulfide catalyst based on mesoporous aluminosilicate Al-HMS-10.

The following chemicals were used for preparing mesoporous aluminosilicate Al-HMS-10 (here 10 is the Si/Al atomic ratio): tetraethoxysilane (TEOS, 98%, Sigma-Aldrich), hexadecylamine (HDA, 90%, Sigma-Aldrich), aluminum *sec*-butoxide (97%, Sigma-Aldrich), and isopropyl alcohol (IPA, Komponent-Reaktiv). The synthesis procedure and characteristics of the material are described elsewhere [12].

The metals were applied by impregnation of the support with a solution of their salts in aqueous citric acid (chemically pure grade, Khimreaktiv, Russia). As starting transition metal compounds we used ammonium paramolybdate tetrahydrate  $(\text{NH}_4)_6\text{Mo}_7\text{O}_{24} \cdot 4\text{H}_2\text{O}$  (99%, Alfa Aesar) and nickel nitrate hexahydrate  $\text{Ni}(\text{NO}_3)_2 \cdot 6\text{H}_2\text{O}$  (97%, Sigma-Aldrich). The salts for preparing the solutions were taken in an amount corresponding to the Ni and Mo content of the catalyst of 7 and 24 wt %, respectively. The thickness of the liquid layer over the support after adding the impregnation solution did not exceed 2 mm. The samples were left overnight for the impregnation, after which the solution was decanted. The materials were dried in the temperature interval  $80\text{--}110^\circ\text{C}$  (for 1 h at each temperature) and then were calcined in a muffle furnace in air for 2 h at  $350^\circ\text{C}$  and for 4 h at  $550^\circ\text{C}$ . As a result, we obtained a catalyst of the composition  $\text{NiO-MoO}_3/\text{Al-HMS-10}$ .

The catalyst was converted to the sulfide form by treatment with elemental sulfur (chemically pure grade, Khimreaktiv) at  $350^\circ\text{C}$  and  $\text{H}_2$  pressure of 5 MPa for 5 h. The catalyst of the composition  $\text{NiS-MoS}_2/\text{Al-HMS-10}$  was filtered off, washed with toluene (ultrapure grade,

**Table 1.** Reactant ratios and amounts

Catalyst	Mo : substrate	$\omega(S)$ , wt %	Mo : Ni	$\omega(\text{substrate})$ , wt %	CO/H <sub>2</sub> O	$\omega(\text{H}_2\text{O})$ , wt %
Unsupported Ni–Mo sulfide catalyst	1 : 14	2.5	3 : 1	10	1.5	20
NiS–MoS <sub>2</sub> /Al-HMS-10	1 : 12	–				

Khimmed, Russia), and dried for 2 h at 60°C in an inert atmosphere.

**Catalytic experiments.** The catalytic experiments on hydrogenation of sulfones were performed in a steel autoclave with continuous stirring of the reaction mixture. The temperature in the reactor was maintained with a resistance furnace equipped with a thermocouple and a temperature controller. The reaction was performed in the presence of Ni–Mo sulfide catalysts supported on mesoporous aluminosilicate Al-HMS and of unsupported catalysts prepared in situ by thermal composition of poorly soluble precursors. As such precursors we chose molybdenum hexacarbonyl Mo(CO)<sub>6</sub> (99.99%, Sigma–Aldrich) and nickel(II) naphthenate Ni(C<sub>10</sub>H<sub>7</sub>COO)<sub>2</sub> (5–12 wt % Ni, Sigma–Aldrich). In the case of unsupported systems, the catalytically active particles were formed directly in the course of hydrogenation. To form the active phase of the catalyst (molybdenum sulfide), 2.5 wt % elemental sulfur (chemically pure grade, Khimreaktiv) was additionally introduced into the reaction mixture. The molybdenum content of the reaction mixture was calculated using the formula

$$\omega_{\text{Mo}} = \frac{m[\text{Mo}(\text{CO})_6]M(\text{Mo})}{M[\text{Mo}(\text{CO})_6]m(\text{solution})} \times 100\%$$

where  $m[\text{Mo}(\text{CO})_6]$  is the molybdenum hexacarbonyl weight (g);  $M(\text{Mo})$ , molybdenum molar weight (96 g mol<sup>-1</sup>);  $M[\text{Mo}(\text{CO})_6]$ ; molybdenum hexacarbonyl molar weight (264 g mol<sup>-1</sup>); and  $m(\text{solution})$ , solution weight (g),  $m(\text{solution}) = m(\text{H}_2\text{O}) + m(\text{solvent}) + m(\text{sulfur})$ .

Hydrogenation of sulfones was performed at elevated CO pressure in the presence of water ensuring in situ generation of hydrogen via water-gas shift reaction [13], with toluene (ultrapure grade, Khimmed) used as solvent. The reactant ratios and amounts are given in Table 1.

**Methods for studying the catalysts.** The specific surface area and the pore volume and diameter were

determined by low-temperature adsorption/desorption of nitrogen with a Micromeritics Gemini VII 2390t device at 77 K. Prior to measurements, the samples were degassed at 310°C for 6 h. The specific surface area was calculated by the Brunauer–Emmett–Teller method from the adsorption data in the relative pressure interval  $p/p_0 = 0.04\text{--}0.20$ . The pore volume and size distribution were determined from the adsorption branch of the isotherms using the Barrett–Joyner–Halenda model. The specific pore volume was calculated from the amount of the adsorbed nitrogen at a relative pressure  $p/p_0 = 0.99$ . The normalized specific surface area of the oxide form of the catalyst was calculated from the formula

$$NS_{\text{BET}} = \frac{S_{\text{BET catalyst}}}{[(1-y)S_{\text{BET support}}]},$$

where  $y$  is the content of the metals (wt %).

The metal content of the samples was determined quantitatively by inductively coupled plasma atomic emission spectroscopy (AES-ICP) with an IRIS Interpid II XPL (Thermo Electron, the United States) with radial and axial observation at a wavelength of 343.49 nm.

The structure and morphology of the catalyst surfaces were examined with a Jeol Jem analytical electron microscope at magnifications from 80 to 500 000 and image resolution of 0.2–0.34 nm.

The acidity of the materials was determined with a Micromeritics AutoChem HP chemisorption analyzer. The samples was crushed to a particle size of 1–2 mm, placed in a reactor, and calcined in a helium flow at 400°C for 30 min, after which the temperature was decreased to 100°C and the sample was saturated with ammonia for 30 min. Physically adsorbed ammonia was removed in a helium stream until the baseline drift stopped. Then, the reactor was heated to 750°C at a rate of 20 deg min<sup>-1</sup>. The amount of ammonia desorbed in the course of TPD was calculated using the AutoChem HP V2.04 program.

**Table 2.** Textural characteristics of mesoporous aluminosilicate and catalyst based on it

Sample	$S_{\text{BET}}, \text{m}^2 \text{g}^{-1}$	$D_{\text{pore}}, \text{\AA}$	$V_{\text{pore}}, \text{cm}^3 \text{g}^{-1}$
Al-HMS-10	773	45	0.88
NiO–MoO <sub>3</sub> /Al-HMS-10	456	42	0.76

**Analysis of reaction products.** The sulfone hydrogenation products were analyzed with a Kristall-Lyuks4000M gas–liquid chromatograph equipped with a flame ionization detector and a PetrocolTM (Supelco) 0.25 mm × 30 m capillary column under the conditions of programmed heating. The carrier gas was helium.

## RESULTS AND DISCUSSION

Hydroconversion of sulfones was performed in the presence of Ni–Mo sulfide catalysts based on mesoporous aluminosilicate or of catalysts formed in situ in the reaction medium. Mesoporous aluminosilicate Al-HMS-10 was used as a support for Ni–Mo sulfide catalysts. The preparation procedure, structure, and characteristics of the material are described elsewhere [12]. Catalysts on this support have high specific surface area and the pore size ensuring the substrate access to the active component. Therefore, they show high performance in hydrogenation.

The standard procedure for applying metals is im-

pregnation of the support with solutions of their salts. In this step, the Ni and Mo compounds interact with the porous system of the support, which determines their morphology and composition of the active phase of the catalyst. The use of chelating agents favors uniform distribution of the metals on the support surface and formation of the catalytically active Ni–Mo–S phase [14]. Citric acid was used as a chelating agent. Bimetallic complexes of the composition  $[\text{Ni}(\text{H}_2\text{O})_2]_2[\text{Mo}_4\text{O}_{11}(\text{C}_6\text{H}_5\text{O}_7)_2]$  are formed in the impregnation system when using solutions of Ni and Mo salts in citric acid. In the course of subsequent drying and calcination, these complexes decompose with the formation of oxides of the corresponding metals on the support surface.

As found by AES-ICP, the content of NiO and MoO<sub>3</sub> in terms of the metal is 6 and 22 wt %, respectively, which is close to the calculated values.

According to the low-temperature nitrogen adsorption/desorption data, the specific surface area of the materials and the pore diameter decrease on applying the metals (Table 2).

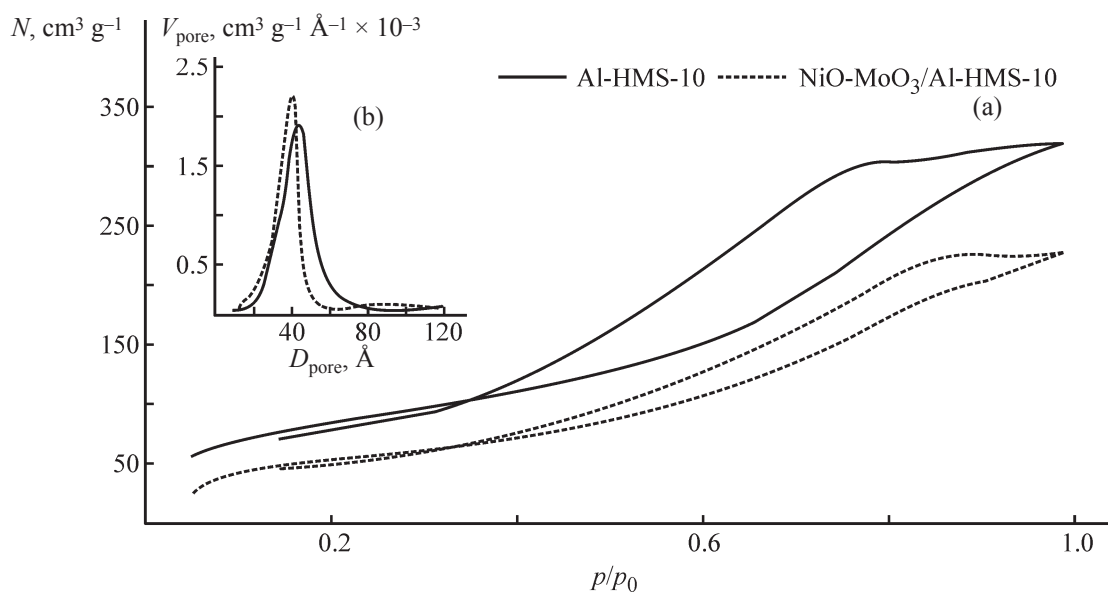


**Fig. 2.** (a) Nitrogen adsorption/desorption isotherms and (b) pore size ( $D_{\text{pore}}$ ) distribution for mesoporous aluminosilicate and Ni–Mo catalyst based on it. ( $N$ ) Amount of desorbed nitrogen, ( $V_{\text{pore}}$ ) pore volume, and ( $p/p_0$ ) relative pressure.

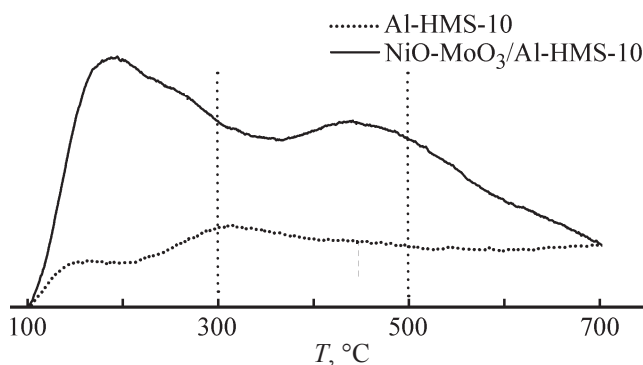


**Fig. 3.** Profiles of  $\text{NH}_3$  TPD curves for aluminosilicate Al-HMS and oxide form of the Ni-Mo catalyst. ( $T$ ) Temperature.

However, the mesoporous structure of the materials is preserved, as indicated by the hysteresis loop of type IV in the nitrogen adsorption/desorption curves (Fig. 2). The mesoporous structure of the materials is confirmed by capillary adsorption of nitrogen in pores at the relative pressure  $p/p_0 = 0.35$ .

The quantity  $NS_{\text{BET}}$  for the catalyst exceeds 0.8, suggesting that the pores on applying the metals are blocked insignificantly.

The acidity of the aluminosilicate and catalyst based on it were evaluated by TPD of  $\text{NH}_3$  (Fig. 3).

All the curves were analyzed using the Gauss-Lo-rentz approximation method. The acid sites were subdivided with respect to the temperature range of ammonia desorption into weak ( $T < 300^\circ\text{C}$ ), medium-strength ( $T = 300\text{--}500^\circ\text{C}$ ), and strong ( $T > 500^\circ\text{C}$ ). The concentrations of the acid sites, expressed in micromoles of the desorbed  $\text{NH}_3$  per gram of the catalyst, are given in Table 3.

According to the TPD- $\text{NH}_3$  data, the amount of medium-strength acid sites decreases upon application of the metals with an increase in the fraction of strong acid sites. The total acidity of the materials decreases by  $60 \mu\text{mol g}^{-1}$ .

The support strongly influences the catalyst morphology. For example, Mo-O-Al bonds can be formed in the mesoporous aluminosilicate, leading to the predominant formation of monolayer  $\text{MoS}_2$  sheets in the course of sulfiding. In the case of supported catalysts, smaller number of sulfide layers in the stack may also be due to weak interaction of metal sulfides with silicon present in the support [15–17]. In the case of dispersed unsupported catalysts, the catalytically active phase is formed directly in the reaction medium. Therefore, the reaction parameters influence its composition and structure.

The layered packing of  $\text{MoS}_2$  particles is clearly seen in the TEM images of the  $\text{NiS-MoS}_2/\text{Al-HMS-10}$  catalyst and catalyst formed in situ by decomposition of insoluble precursors and separated from the reaction mixture immediately after the reaction (Figs. 4a, 4b, respectively).

The active component in the samples of the sulfide catalysts obtained consists of multilayer bent stacks of molybdenum sulfide. Its formation is also proved by the interplanar spacing of  $4.4 \text{ \AA}$ , corresponding to the basal (002) plane of  $\text{MoS}_2$  crystallites. Statistical analysis of the TEM images of sulfide catalysts shows that the mean length of the active phase particles on the surface of the catalyst supported on Al-HMS-10 is 3–5 nm, and the mean number of layers in the stack is 3.

Unsupported Ni-Mo sulfide catalysts formed in situ in the reaction medium are characterized by high content of the active phase and, as a consequence, by high activity in hydrogenation. In such catalytic systems, the effect of steric and diffusion factors hindering the access of the substrate to the active component of the catalyst is virtually fully eliminated. The choice of oil-soluble precursors is governed by the fact that they readily dissolve in hydrocarbons and form highly catalytically active nanoparticles in the

**Table 3.**  $\text{NH}_3$  TPD data for samples of aluminosilicates and catalysts based on them

Sample	Weak acid sites <sup>a</sup>	Medium-strength and strong acid sites <sup>b</sup>	Total ammonia amount
	$\mu\text{mol g}^{-1}$		
Al-HMS-10	95	318	413
NiO-MoO <sub>3</sub> /Al-HMS-10	115	238	353

<sup>a</sup> Amount of ammonia desorbed up to  $300^\circ\text{C}$ .

<sup>b</sup> Amount of ammonia desorbed above  $300^\circ\text{C}$ .

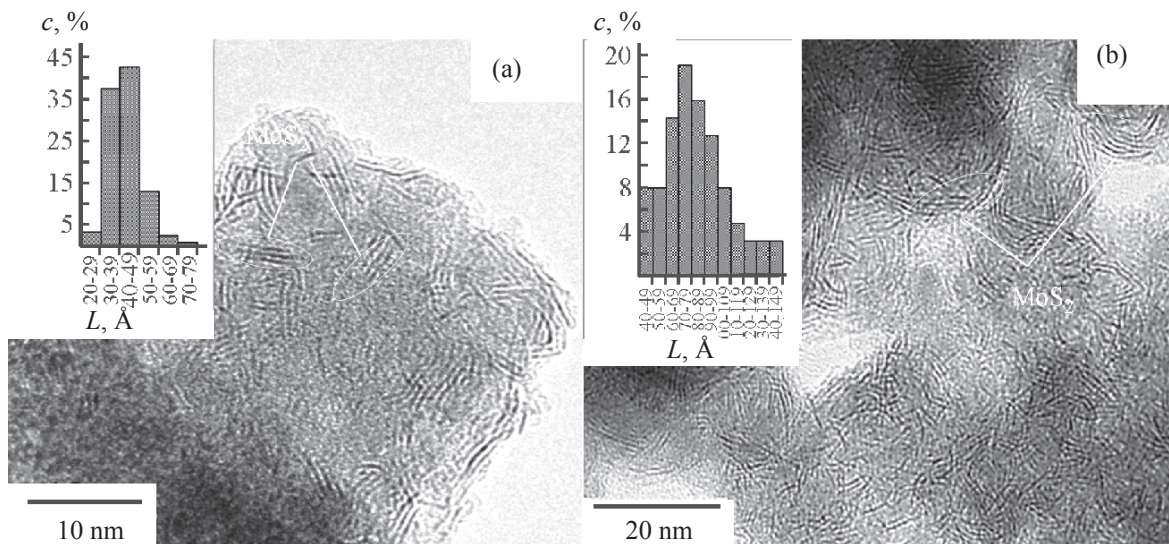


**Fig. 4.** TEM images and length ( $L$ ) distribution of sulfide particles for the (a) NiS–MoS<sub>2</sub>/Al-HMS-10 catalyst and (b) unsupported Ni–Mo sulfide catalyst. (c) Content.

course of thermal decomposition in the presence of a sulfiding agent. The mean length of active component particles in the unsupported dispersed Ni–Mo sulfide catalyst prepared in the reaction medium is 6–9 nm, and the mean number of active component layers in the multilayer agglomerate is 4.0. Molybdenum sulfide crystallites of length larger than 10 nm are also formed; their fraction is about 22%.

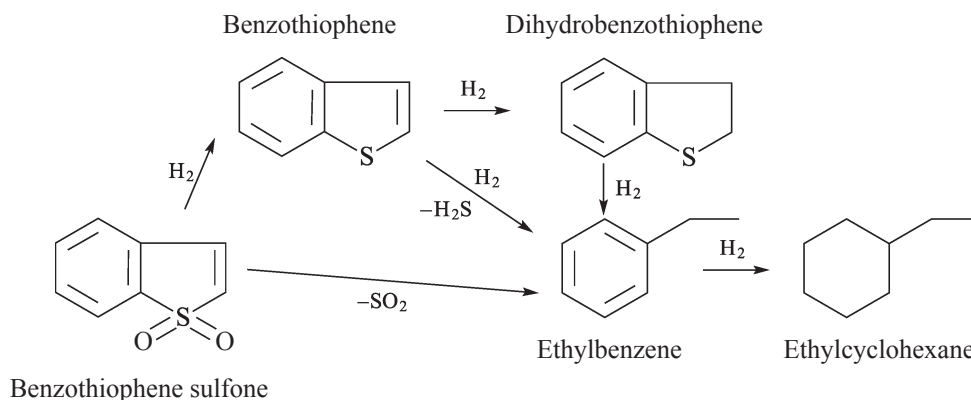
Under the conditions of hydroprocesses, sulfones can undergo thermal cracking or hydrogenation to the corresponding benzothiophenes [18]. Hydroconversion of the latter compounds can occur as hydrogenation of the benzene ring, followed by elimination of hydrogen sulfide, or as direct hydrogenolysis of the C–S bond (Scheme 1). In the case of benzothiophene, thermal cracking leads to the formation of ethylbenzene, which

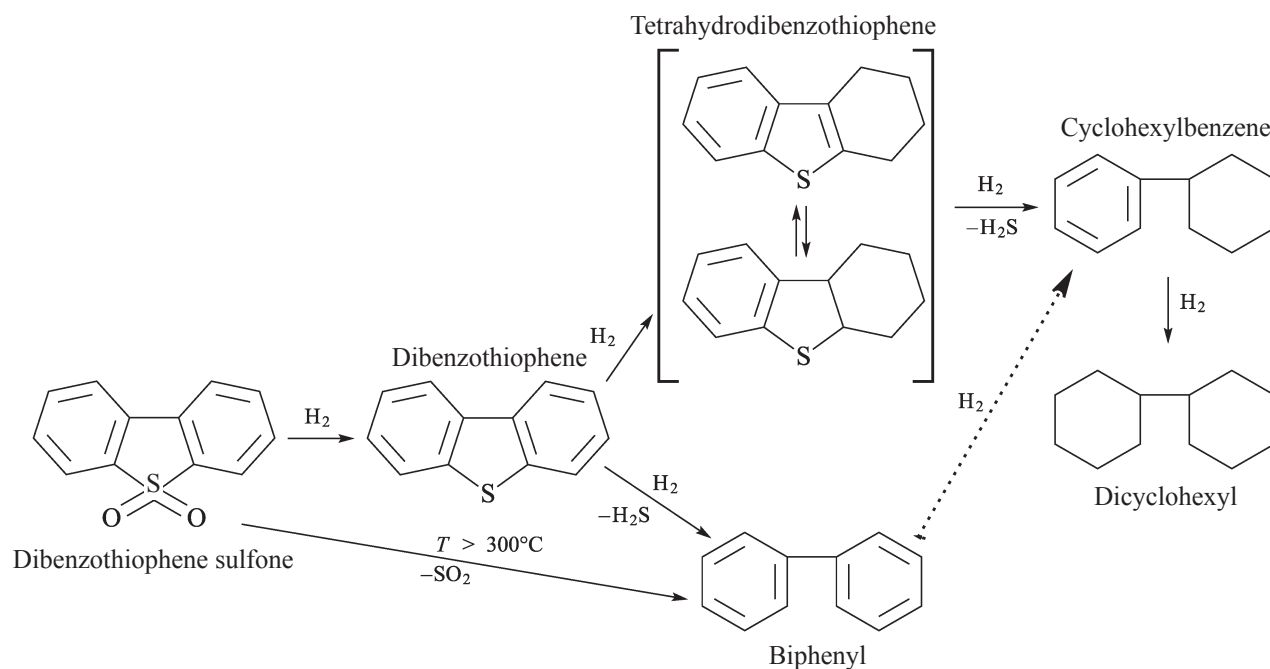
can also be formed via hydrogenation or desulfurization of benzothiophene.

Thermal cracking of dibenzothiophene sulfone ( $T > 300^\circ\text{C}$ ) yields biphenyl. The occurrence of the reaction along the sulfone hydrogenation pathway leads to the accumulation of dibenzothiophene in the reaction mixture. This compound undergoes hydrogenolysis of the C–S bond with the formation of biphenyl or takes up hydrogen to form tetrahydrodibenzothiophene and cyclohexylbenzene (Scheme 2).

Hydrogenation of benzothiophene sulfone in the presence of unsupported Ni–Mo sulfide catalyst at 250 and 350°C for 4 h leads to the formation of benzothiophene whose yield does not exceed 30%. An increase in the reaction time to 6 h leads to the formation of trace amounts (no more than 7%) of ethylbenzene (Fig. 5).

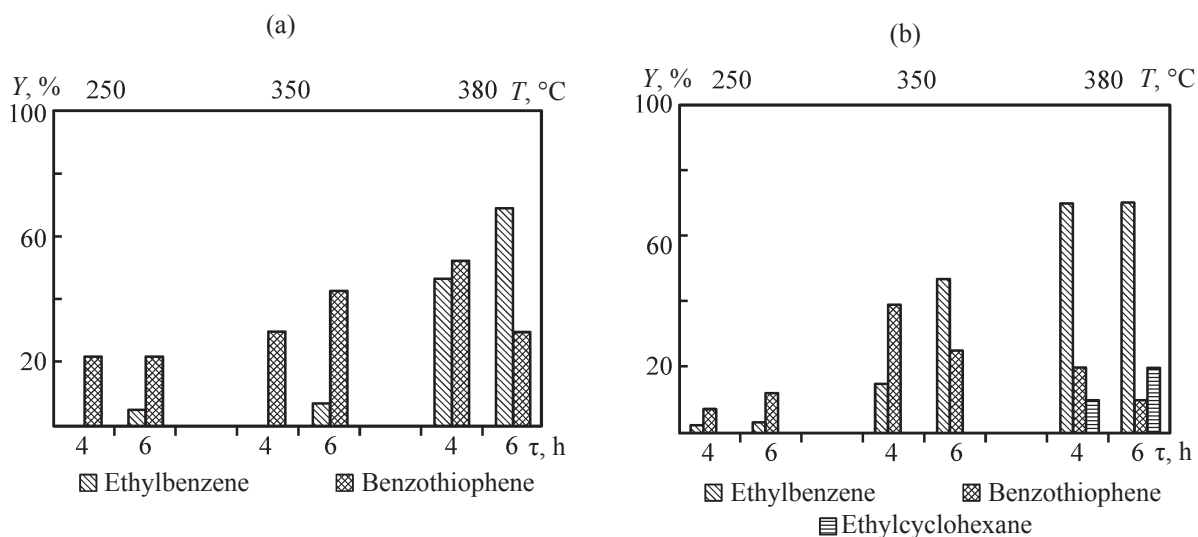
**Scheme 1.** Benzothiophene sulfone transformations under the conditions of hydroprocesses.



**Scheme 2.** Dibenzothiophene sulfone transformations under the conditions of hydroprocesses.

Further temperature elevation to  $350^{\circ}\text{C}$  allows reaching quantitative conversion of benzothiophene sulfone. The ethylbenzene content increases to 47 and 70% when performing the reaction for 4 and 6 h, respectively. Throughout the examined temperature interval, no ethylcyclohexane, which could be formed by complete hydrogenation of benzothiophene, was detected in the reaction products.

The catalyst supported on mesoporous aluminosilicate Al-HMS-10 is less active at  $250^{\circ}\text{C}$ : The benzothiophene sulfone conversion does not exceed 15% even after the 6-h reaction. The temperature elevation leads to a significant increase in the conversion, which at  $380^{\circ}\text{C}$  becomes quantitative already in 4 h. In this case, ethylcyclohexane is formed with 20% selectivity.

**Fig. 5.** Distribution of products of benzothiophene sulfone hydrogenation in the presence of (a) unsupported Ni-Mo sulfide catalyst and (b) catalyst based on mesoporous aluminosilicate Al-HMS-10. (Y) Yield, (T) temperature, and ( $\tau$ ) time; the same for Fig. 6.

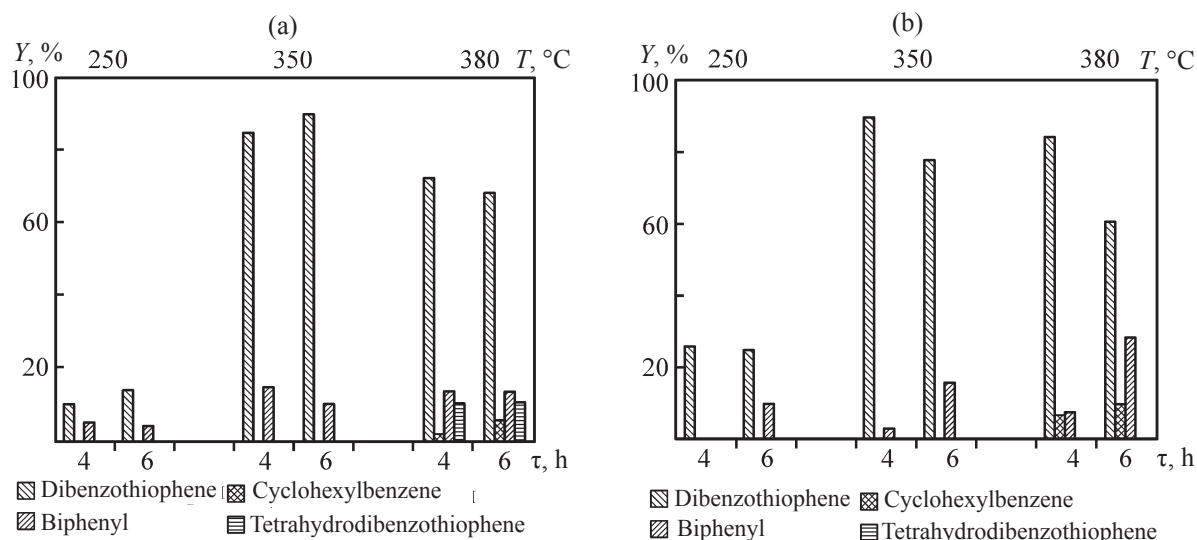


**Fig. 6.** Distribution of products of dibenzothiophene sulfone hydrogenation in the presence of (a) unsupported Ni–Mo sulfide catalyst and (b) catalyst based on mesoporous aluminosilicate Al-HMS-10.

Lower activity of catalysts supported on Al-HMS in hydrogenation of benzothiophene may be due to partial blocking of pores upon application of the metals (according to the calculations of the normalized BET specific surface area for the oxide form of the catalyst), so that the active sites of the catalyst become less accessible to substrate molecules. Furthermore, introduction of aluminum into the silicate structure can lead to the formation of Mo–O–Al bridging bonds and, as a consequence, to the formation of NiMoS of type I. However, this phenomenon is leveled out by high specific surface area of the mesoporous material and its high adsorption capacity for sulfur compounds, caused by the presence of aluminum atoms bound to the surface hydroxy groups.

The catalyst activity in dibenzothiophene hydrogenation is determined by the number of molybdenum sulfide layers in the agglomerate. This characteristic determines the steric hindrance to adsorption of a substrate molecule on active sites of the catalyst. An increase in the number of layers in the MoS<sub>2</sub> packing leads to an increase in the number of edge and vertex sites and, as a consequence, to high activity of the catalyst. Because the numbers of sulfide layers in the MoS<sub>2</sub> crystallite in the catalysts used is virtually equal, their activities are comparable.

Hydrogenation of dibenzothiophene sulfone under these conditions occurs with high selectivity with respect to dibenzothiophene. With the unsupported Ni–Mo

sulfide catalyst, the quantitative conversion is reached at 350 °C, with 10–15% yield of biphenyl (Fig. 6).

An increase in the temperature to 380 °C leads to the appearance of tetrahydrodibenzothiophene in the reaction products. Its content reaches 11%. This fact suggests that the reaction occurs along the pathway of the aromatic ring hydrogenation followed by hydrogen sulfide elimination. In the process, trace amounts ( $\leq 6\%$ ) of cyclohexylbenzene are formed.

The catalysts supported on mesoporous Al-HMS exhibit higher activity. For example, at 250 °C the conversion of benzothiophene sulfone reaches 35% in 6 h, whereas with the unsupported dispersed catalysts the conversion does not exceed 18%. However, at 380 °C the activity of both kinds of catalysts becomes comparable, with the fraction of dibenzothiophene hydrogenation products reaching 39 and 36%, respectively.

## CONCLUSIONS

Hydroconversion of sulfones to the corresponding benzo- and dibenzothiophenes occurs considerably faster than the subsequent hydrogenation of these products. Therefore, the products that are formed by oxidation of organic sulfur compounds and remain in the hydrocarbon medium (mainly sulfones) will not significantly affect the subsequent hydrotreatment because under the conditions of hydroprocesses they transform into the corresponding benzo- and dibenzothiophenes, which

undergo the subsequent hydrodesulfurization to form mono- and diaromatic hydrocarbons.

#### ACKNOWLEDGMENTS

The study was financially supported by the Ministry of Education and Science of the Russian Federation within the framework of the Federal Target Program “Research and Development in Priority Directions of the Progress of the Scientific and Technological Complex of Russia for the Period 2014–2020,” measure 1.3, subsidizing agreement no. 14.607.21.0173 of September 26, 2017, unique applied research identifier RFMEFI60717X0173.

#### REFERENCES

1. Fang, Y. and Hu, H., *Catal. Commun.*, 2007, vol. 8, no. 5, pp. 817–820.
2. Zhou, X., Zhao, C., Yang, J., and Zhang, S., *Energy Fuels*, 2007, vol. 21, no. 1, pp. 7–10.
3. Yukari, Y., Yasutaka, K., and Yasuyuki, U., *Eur. J. Inorg. Chem.*, 2014, vol. 2014, no. 25, pp. 4073–4078.
4. Tang, N., Jiang, Z., and Li, C., *Green Chem.*, 2015, vol. 17, no. 2, pp. 817–820.
5. Ma, X., Zhou, A., and Song, C., *Catal. Today*, 2007, vol. 123, no. 1, pp. 276–284.
6. Zhang, W., Zhang, H., Xiao, J., et al., *Green Chem.*, 2014, vol. 16, no. 1, pp. 211–220.
7. Lu, M.-C., Biel, L.C.C., Wan, M.-W., et al., *Int. J. Green Energy*, 2014, vol. 11, no. 8, pp. 833–848.
8. Campos-Martin, J.M., Capel-Sanchez, M.C., Perez-Presas, P., and Fierro, J.L.G., *J. Chem. Technol. Biotechnol.*, 2010, vol. 85, no. 7, pp. 879–890.
9. Akopyan, A.V., Ivanov, E.V., Polikarpova, P.D., et al., *Petrol. Chem.*, 2015, vol. 55, no. 7, pp. 571–574.
10. Abro, R., Abdeltawab, A.A., Al-Deyab, S.S., et al., *RSC Adv.*, 2014, vol. 4, no. 67, pp. 35302–35317.
11. Etemadi, O. and Yen, T.F., *Energy Fuels*, 2007, vol. 21, no. 3, pp. 1622–1627.
12. Vutolkina, A.V., Glotov, A.P., Egazar'yants, S.V., et al., *Chem. Technol. Fuels Oils*, 2016, vol. 52, no. 5, pp. 515–526.
13. Vutolkina, A.V., Makhmutov, D.F., Zanina, A.V., et al., *Nanoheterogeneous Catal. (Appl. Petrol. Chem.)*, 2018, vol. 3, no. 1, pp. 12–17.
14. Calderón-Magdaleno, M.Á., Mendoza-Nieto, J.A., and Klimova, T.E., *Catal. Today*, 2014, vol. 220, pp. 78–88.
15. Ninh, T.K.T., Massin, L., Laurenti, D., and Vrinat, M., *Appl. Catal. A: General*, 2011, vol. 407, pp. 29–39.
16. Ding, L., Zheng, Y., Zhang, Z., and Ring, Z., *Appl. Catal. A: General*, 2007, vol. 319, pp. 25–37.
17. Roukoss, C., Laurenti, D., Devers, E., et al., *Compt. Rend. Chim.*, 2009, vol. 12, pp. 683–691.
18. Kim, M.J., Kim, H., Jeong, K., et al., *J. Ind. Eng. Chem.*, 2010, vol. 16, pp. 539–545.